[37]L. J. Vieland, R. W. Cohen, and W. Rehwald, Phys. Rev. Letters 26, 373 (1971).

[38]I am indebted to Dr. L. J. Vieland for bringing Ref. 12 to my attention.

[39]S. Barisic, J. Labbé, and J. Friedel, Phys. Rev. Letters 25, 919 (1970).

[40]S. Barisic (unpublished).

[41]A. B. Migdal, Zh. Eksperim. i Teor. Fiz. 34, 1438 (1958) [Sov. Phys. JETP 7, 996 (1958)].

[42]In Ref. 15 the special case $G_{12} = -\frac{1}{2} G_{11}$ was considered.

[43]Low-frequency ultrasonic experiments measure the adiabatic elastic constants. In the cubic phase the isothermal and the adiabatic elastic constants are equal. They are also equal at $T = 0$. For intermediate temperatures the two sets of elastic constants are somewhat different.

[44]Compare Ref. 29.

[45]$(C_{11})_{av} = \frac{1}{3}(2C_{11} + C_{33})$, $(C_{12})_{av} = \frac{1}{3}(2C_{13} + C_{12})$.

PHYSICAL REVIEW B VOLUME 4, NUMBER 4 15 AUGUST 1971

Generalized Susceptibility Function for Rare Earths and Thorium and Their Alloys*

S. H. Liu, R. P. Gupta, and S. K. Sinha
Institute for Atomic Research and Department of Physics, Iowa State University, Ames, Iowa 50010

(Received 25 February 1971)

The results of calculations of the generalized susceptibility function $\chi(\vec{q})$ for the rare-earth metals and thorium and its alloys with rare earths are presented. For the heavy rare earths Gd, Tb, Dy, Er, and Lu, the calculation was confined to the ΓA direction, and a mesh of 450 000 points in the Brillouin zone was used. For the double-hexagonal close-packed crystals Nd and Pr, a mesh of 400 000 points in the Brillouin zone was chosen, while for thorium and its fcc alloys with rare earths, a mesh of 2 048 000 points in the Brillouin zone was used. The results of calculations on Sc and Y have also been included for the sake of comparison with the heavy rare earths. The matrix elements, which couple the f electron and the conduction electron, appearing in the expression for the generalized susceptibility function, were taken to be constant. Our calculations show that the $\chi(\vec{q})$ curves obtained in this way are reasonably smooth and the scatter of points along the curves is less than 3%. The results have been compared with the experimental data on turn angles, spin-wave dispersion curves, and phonon spectra where available.

I. INTRODUCTION

The rare earths form a class of metals which exhibit fascinating magnetic structures below characteristic transition temperatures. In general, most heavy rare earths, with which we shall be chiefly concerned in this paper, have been found to exist in antiferromagnetic phases with a sinusoidal, a spiral, or a more complex arrangement of magnetic moments which are periodic with the periodicity along the c axis.[1] The electronic configuration of these metals is described by a set of closed shells containing 54 electrons corresponding to xenon, a partially filled $4f$ shell, and three electrons in the $5d$ and $6s$ states. The $4f$ electrons are highly localized and retain their orbital moment, as indicated by the data on entropy and magnetic properties. The $5d$ and $6s$ electrons are itinerant, as expected. Because of the high degree of localization of $4f$ electrons, there is practically no overlap between the neighboring ion cores, the nearest-neighbor distance being on the average 10 times the ionic radius. The principal mechanism responsible for magnetic ordering is believed to be the indirect exchange in which the conduction electrons play a key role to help neighboring ions interact with each other. The idea is that each $4f$ shell moment polarizes the spins of the conduction electrons in the neighborhood of the ion through an exchange interaction. The conduction electrons respond with an oscillatory and long-range polarization, and this in turn aligns a number of other f moments within the range.

The theory of indirect exchange interaction was first developed by Ruderman and Kittel[2] for the case of nuclei interacting via the hyperfine interaction with the conduction electrons. Kasuya[3] and Yosida[4] extended these ideas and obtained the so-called Ruderman-Kittel-Kasuya-Yosida (RKKY) exchange interaction for magnetic materials such as rare earths where there is almost no direct overlap between the magnetic ions.[5–8] It is assumed in this theory that the interaction of the Heisenberg $\vec{S}\cdot\vec{s}$ type between the f spin $\vec{S}$ and the conduction electron spin $\vec{s}$ is valid. This con-

dition is, of course, not precisely met in the case of rare earths because of the orbital contribution to the magnetic moment, as pointed out by Elliott and Thorpe.[9] The interaction depends upon: (a) the exchange integral between localized ionic cores and the conduction-electron wave functions at the ionic sites; and (b) the energy bands and Fermi surface of conduction electrons. The latter is related to the $\vec{q}$-dependent generalized susceptibility function $\chi(\vec{q})$, which is the response of the conduction electrons in the metal to the effective field of the ionic moments, through its Fourier transform, as shown by Kubo[10] in the linear-response approximation. The interaction energy of the system is, in fact, proportional to the negative of the susceptibility function.[11]

Obviously, the generalized susceptibility function $\chi(\vec{q})$ is an important quantity in the determination of the magnetic structure. The maximum in $\chi(\vec{q})$ fixes the minimum in the exchange energy and hence determines the wave vector $\vec{q}$ which will be assumed at the ordering temperature. The maximum in $\chi(\vec{q})$ is, however, not a sufficient condition for the magnetic ordering to occur. Whether or not the substance will order magnetically will depend upon the relative importance of the exchange energy term in the free-energy expression. If the exchange-energy term happens to be the dominant contribution, then the substance will exhibit magnetism. A peak in $\chi(\vec{q})$ at $\vec{q}=0$ would then mean ferromagnetism, and the one at some other $\vec{q}$ would indicate a sinusoidal, a helical, or a more complicated arrangement of magnetic moments with a period defined by that wave vector. In what follows, we discuss some of the approximations which are usually made in the calculation of $\chi(\vec{q})$. The $\chi(\vec{q})$ is given by the following expression:

$$\chi(\vec{q}) = -\frac{1}{N}\sum_{k,k'}\frac{n_k - n_{k'}}{E_k - E_{k'}} I^2(k,k')\,\delta_{\vec{k}',\vec{k}+\vec{q}+\vec{H}}\,, \qquad (1)$$

where k includes both the wave vector $\vec{k}$ and the band index; $\vec{H}$ is a reciprocal lattice vector necessary to bring the sum $\vec{k}+\vec{q}$ back to the first Brillouin zone; and $I(k,k')$ is a matrix element which depends both on the wave functions of the conduction electrons and the localized f electrons. The approximations which have usually been introduced in the calculation of $\chi(\vec{q})$ are: (a) to ignore the dependence of the matrix element $I(k,k')$ on k and k' and consider it to be a function independent of k, k' and $\vec{q}$; and (b) to assume nearly-free-electron-like Fermi surface and energy bands. Under these assumptions, Eq. (1) takes on a simple well-known form

$$\chi(\vec{q}) = I^2\frac{3}{2E_F}\left(\frac{1}{2} + \frac{1-t^2}{4t}\ln\left|\frac{1+t}{1-t}\right|\right)\,, \qquad (2)$$

with $t = q/2k_F$, where k_F is the Fermi wave vector. Notice that $\chi(\vec{q})$, in the above approximations, is an isotropic function (as is the Fermi surface in this approximation) and depends only on the magnitude of the wave vector $\vec{q}$.

Recently, the band calculations of Dimmock and Freeman,[12] Freeman *et al.*,[13] and Keeton and Loucks[14,15] for the heavy rare earths have shown that the Fermi surfaces of these metals are extremely anisotropic and bear no relation to the ones calculated in the nearly-free-electron approximation. A general feature which was found characteristic of these Fermi surfaces is that they possessed nearly flat parallel regions perpendicular to the c axis. Keeton and Loucks[14] stressed that the wave vector separating these surfaces is precisely the one where the $\chi(\vec{q})$ will have a maximum and hence will determine the magnetic $\vec{q}$. They successfully attempted to relate the dimensions of their calculated Fermi surfaces with the experimental data on turn angles. Roth *et al.*[16] had previously discussed the relation between $\chi(\vec{q})$ and the geometry of the Fermi surface but made no application to any specific metal.

Evenson and Liu[17–19] were the first to calculate the $\chi(\vec{q})$ for several heavy rare earths using the bands calculated by Keeton and Loucks[14] by the relativistic augmented-plane-wave (RAPW) method. They were able to obtain a fairly good agreement between the calculated and experimental wave vectors for ordering. A mesh of about 27 000 points was used in their calculation. An unexpected feature of their calculation was that, although it was possible to draw a smooth curve through the calculated points, the points nevertheless showed a considerable scatter around the curve. In order to examine the cause of such a noise, a numerical calculation of $\chi(\vec{q})$ for spherical and cubic Fermi surfaces was performed and the results compared with those obtained analytically.[18] It was found that the scatter in the calculation was chiefly due to the coarseness of the mesh. In a coarse mesh the Fermi surface no longer looks smooth, but rather appears to consist of a series of parallel steps, the width of each step depending upon the coarseness of the mesh. Such a distortion of the Fermi surface obviously gives rise to spurious peaks in $\chi(\vec{q})$.

The purpose of this paper is to report the results of our calculation for the heavy rare earths Gd, Tb, Dy, Er, and Lu in the c direction. The mesh used in these calculations is considerably finer than the one used by Evenson and Liu.[18] The $\chi(\vec{q})$ of light rare earths Nd and Pr have also been recalculated using a much finer mesh than the one used by Fleming and Liu.[20,21] The results for thorium and its alloys with rare earths, which have an fcc crystal structure, are also reported. The

indirect exchange theory is obviously applicable for such alloys because there is no overlap between the magnetic ions. Results for yttrium and scandium are included for comparison with other rare earths.

II. METHOD OF INTERPOLATION

The mesh in which the energy bands are calculated is generally too coarse to expect meaningful results for $\chi(\vec{q})$. One could, in principle, perform the entire energy-band calculation for a very fine mesh at the outset, but this is a tremendous task which is very tedious in practice. One is therefore forced to employ some sort of interpolation scheme through which reasonable results can be obtained in the expanded mesh. Admittedly the interpolation method will be meaningful only if the initial mesh is not too coarse to expect large errors. The use of a polynomial of some degree is the most commonly employed interpolation scheme. In the present case, one could use a linear or quadratic interpolation which, of course, might not be too bad because of inherent uncertainties in the calculated energy bands themselves. The point, however, is that the interpolated energies should reflect the smoothness of the energy bands and should not add any further errors. The standard way to carry out such an interpolation is by the method of "Spline-fits" which is essentially a piecewise cubic interpolation.[22] The method ensures the continuity not only of the energy bands but also their slopes and their curvatures. In the following, we give a brief outline of this method. Although it is discussed for a one-dimensional chain of points, the interpolation for a three-dimensional case is straightforward and is carried out by making repeated applications of this method.

Let (x_1, y_1), (x_2, y_2), ..., (x_n, y_n) be a linear array of n points arranged in ascending or descending values of x. Let the values of the second derivatives at these points be denoted by g_1, g_2, ..., g_n. Assuming a linear relation, the second derivative g at the point (x, y) lying between (x_k, y_k) and (x_{k+1}, y_{k+1}) is given by

$$g = \frac{g_{k+1} - g_k}{x_{k+1} - x_k}(x - x_k) + g_k \,. \tag{3}$$

On integration the equation of the segment of the curve between x_k and x_{k+1} is found to be the following:

$$y = \frac{(x_{k+1} - x_k)^3}{6d_k} g_k + \frac{(x - x_k)^3}{6d_k} g_{k+1} + c_1 x + c_2 , \tag{4}$$

where $d_k = x_{k+1} - x_k$, and c_1 and c_2 are the constants of integration, which are determined by making use of the fact that the curve passes through the points (x_k, y_k) and (x_{k+1}, y_{k+1}). We thus obtain

$$y = (x_{k+1} - x)^3 \frac{g_k}{6d_k} + (x - x_k)^3 \frac{g_{k+1}}{6d_k} + (x_{k+1} - x) \times (y_k/d_k - \tfrac{1}{6} g_k d_k) + (x - x_k)(y_{k+1}/d_k - \tfrac{1}{6} g_{k+1} d_k) \,. \tag{5}$$

In this equation, all quantities are known except g_k and g_{k+1}, the values of the second derivative at the end points of the segment.

To determine g_k and g_{k+1}, use is made of the fact that the slope of the curve at the point (x_k, y_k) determined from the formula for the interval (x_{k-1}, x_k) must be identical to the one from the formula for the interval (x_k, x_{k+1}). The following

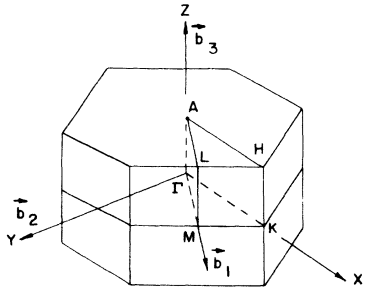

FIG. 1. Brillouin zone for the hexagonal close-packed structure.

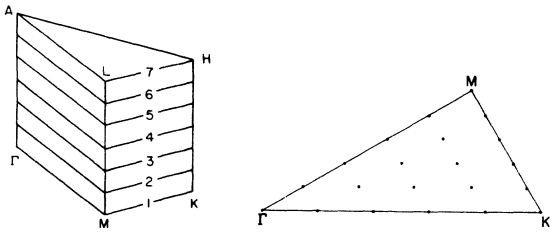

FIG. 2. Initial distribution of points in the irreducible $\frac{1}{24}$th zone.

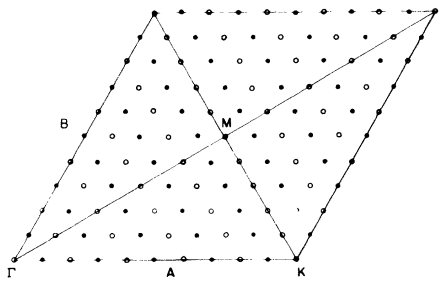

FIG. 3. Basal-plane cross section of the reciprocal space used for interpolation in the case of heavy rare earths.

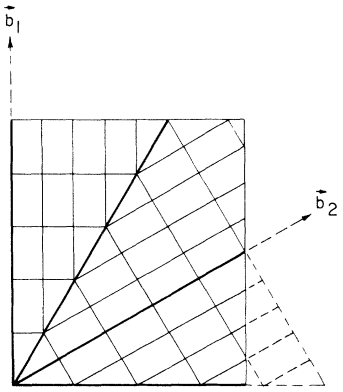

FIG. 4. Basal-plane cross section of the rhombohedron used for interpolation in the case of dhcp metals Nd and Pr.

relation is then obtained:

$$\tfrac{1}{6}d_{k-1}g_{k-1} + \tfrac{1}{3}(d_{k-1}+d_k)g_k + \tfrac{1}{6}d_k g_{k+1} = (y_{k+1}-\gamma_k)/d_k - (y_k - y_{k-1})/d_{k-1} \ . \quad (6)$$

We have such an equation for each interval. There are thus $(n-2)$ equations involving n unknown g's. Two more conditions must be specified to solve this system of simultaneous linear equations. It is usual to put some appropriate constraints on g_1 and g_n such as the values of the second derivative at the end points. In our calculation, it was observed to be most suitable to assume that (a) the slope of the curve is zero at the end points or (b) the second derivative at each end is a linear extrapolation of the value at the two adjacent points. The specific applications of this method to the hexagonal close-packed (hcp), double-hexagonal close-packed (dhcp), and face-centered-cubic (fcc) metals are discussed below.

The heavy rare earths all have the hcp crystal structure. The Brillouin zone for this structure is shown in Fig. 1. There are two atoms in the unit cell and because of this, a phase factor appears in the expression for $\chi(\vec{q})$, which allows the following couplings: (a) within the same band in the first zone; and (b) between adjacent bands from the first to the second zone. In fact, these are precisely the couplings which are obtained in the double-zone representation. The double-zone scheme thus has a distinct advantage over the conventional single zone, and is the most obvious to be employed. The spin-orbit effects, though introducing some complexity, do not present too serious a problem in our calculations, because the splittings on the AHL zone face due to relativistic effects are within the accuracy of the bands.

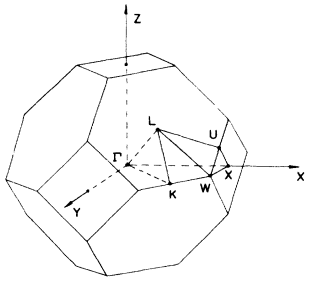

FIG. 5. Brillouin zone for the fcc lattice.

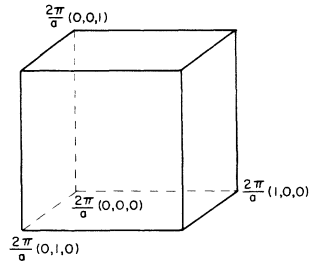

FIG. 6. Section of the reciprocal space used for interpolation in the case of thorium.

As pointed out in Sec. I, the periodicity of magnetic moments in heavy rare earths is along the ΓA direction. The interpolation scheme for calculation of $\chi(\vec{q})$ will therefore be organized for $\vec{q}$ along this direction, although the calculation can be performed for any general direction with only minor modifications in the initial setup. The original mesh used in our calculation consisted of a total of 1800 points in the Brillouin zone.

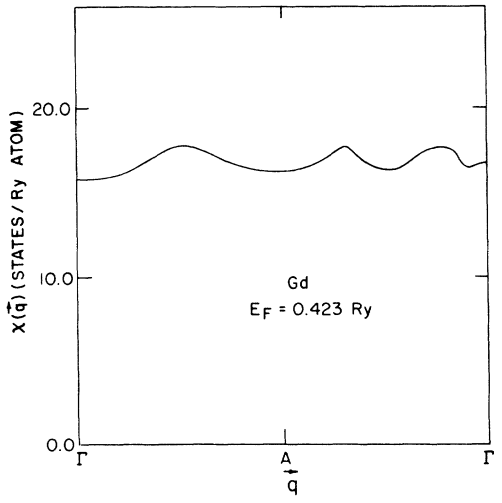

FIG. 7. Generalized susceptibility function for Gd.

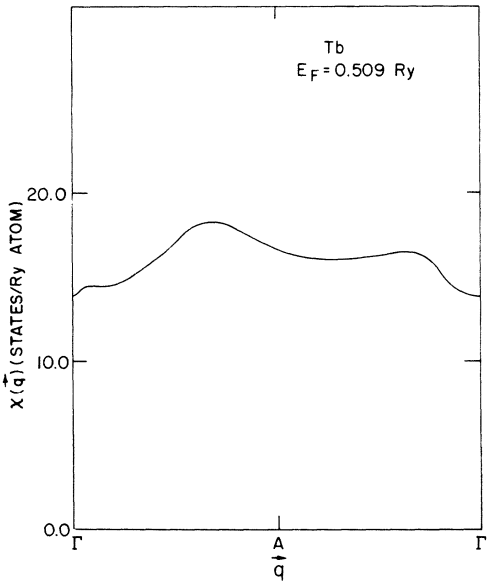

FIG. 8. Generalized susceptibility function for Tb.

The distribution of these points in the irreducible $\frac{1}{24}$th zone is shown in Fig. 2. There are seven equidistant planes which cross ΓA, each containing 21 points.

For convenience a rhombohedral section of the reciprocal space of height $C(=\Gamma A\,\Gamma)$ and volume $\frac{1}{3}$rd of the Brillouin zone was chosen. The base of this rhombohedran is shown in Fig. 3. It was partitioned into 150 000 miniature prisms through a division of its sides A, B, C in, respectively, 50, 50, 60 equal parts, thus obtaining a mesh of 450 000 points in the first Brillouin zone. The distribution of points in the old mesh was, of course, commensurate with the one in the expanded mesh. The results of interpolation were stored on magnetic tape in a set of 51 planes intersecting B, all parallel to the AC plane which contains the ΓA direction; though only the first 26 of them were utilized in the calculation due to considerations of symmetry. Results from only one plane at a time were brought in from the memory locations of the machine and the calculation performed. This process was found to be extremely simple because, for a given $\vec{q}$, $\vec{k}+\vec{q}$ was always to be located in the same plane which contained $\vec{k}$, $\vec{q}$ being, of course, along the ΓA direction. Thus this method eliminated the need for a large amount of storage in the machine.

The light rare-earth metals have a much more complicated crystal structure than the heavy rare earths. Both neodymium and praseodymium, with which we shall be concerned in this paper, have a double-hexagonal close-packed (dhcp) structure. It is formed by stacking the close-packed hexagonal layers in the sequence $ABAC\,ABAC\,\cdots$. For details the reader is referred to the articles by Gschneidner[23] and Pearson.[24] The Brillouin zone for this structure is the same as for the hcp structure. The magnetic structures of Nd and Pr have been determined at Oak Ridge[25,26] by neutron diffraction. The periodicity of the magnetic structure is such that the magnetic wave vector has components both in $\vec{b}_1$ and $\vec{b}_3$ directions. As in the case of heavy rare earths, we choose an original mesh of 147 points in the $\frac{1}{24}$th zone (Fig. 2), but in order to facilitate calculation both in the $\vec{b}_1$ and $\vec{b}_3$ directions and also in the b_1b_3 plane, a rectangular prism of height $4\pi/c\,(=\Gamma A\,\Gamma A\,\Gamma)$, with its base shown in Fig. 4, is chosen. The volume of this prism is obviously one-half that of the Brillouin zone. Each side of the base of the prism is then divided into 50 equal parts and the height of the prism into 80 parts. This division gives an effective mesh of 400 000 in the entire Brillouin zone. For obvious reasons, we have opted to use a quadrupole-zone scheme along the $\vec{b}_3$ direction which eliminates the need for explicit use of phase factors.

For thorium, which crystallizes in an fcc lattice, a starting mesh of 2048 points was chosen in the first Brillouin zone (Fig. 5). A cubic section of the reciprocal space with side $2\pi/a$, as shown in Fig. 6, was found to be the most convenient for the purpose of interpolation. The volume of this cubic section is obviously $\frac{1}{4}$ that of the Brillouin zone. A mesh of 2048 points in the Brillouin zone can be obtained by dividing each side of the cube into eight equal parts, thus partitioning the cube into 512 equal miniature cubes. The side of each miniature cube was further subdivided into 10 equal parts, and thus an effective mesh of 2 048 000 points in the

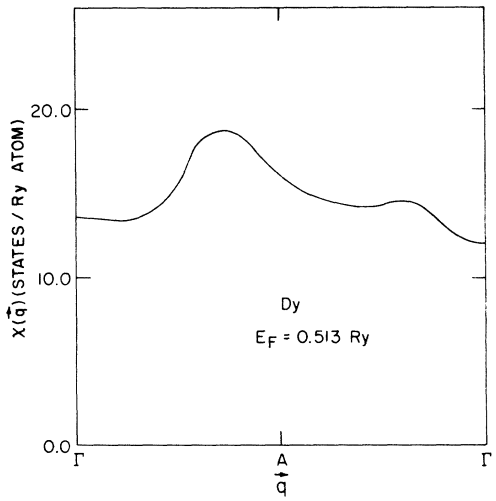

FIG. 9. Generalized susceptibility function for Dy.

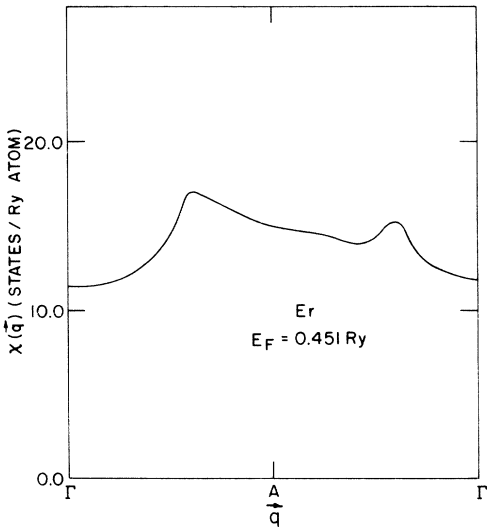

FIG. 10. Generalized susceptibility function for Er.

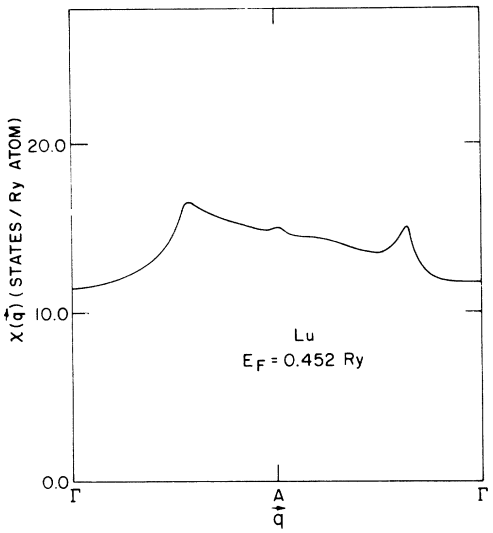

FIG. 11. Generalized susceptibility function for Lu.

Brillouin zone was obtained. The interpolated energies were stored on magnetic tape plane by plane, as in the case of hcp metals, for all the 81 planes perpendicular to the z direction. However, only the first 41 of them were used in the calculation for reasons of symmetry.

III. HEAVY RARE EARTHS

The $\chi(\vec{q})$ curves for the heavy rare earths Gd, Tb, Dy, Er, and Lu are shown in Figs. 7–11 for $\vec{q}$ along the c axis of the hcp crystal. The curves are much smoother than those published previously. The noise level is typically 3%. The Fermi levels given in the graphs are slightly different from those in Ref. 18, and the shift arises from the smoother interpolation. As discussed in Ref. 27 the $\chi(\vec{q})$ curve should be further modified by a matrix element, which is approximated by a function of $\vec{q}$. The effect of this matrix element is to push the right-hand part of the curve downwards. For example, the $\chi(\vec{q})$ for Gd shows a small peak about halfway between Γ and A in the acoustic branch. This peak is definitely not significant because it can be easily removed by the q-dependent matrix element. For Tb, the peak in $\chi(\vec{q})$ is somewhat more pronounced. However, the location of the peak, roughly $0.6\ \pi/c$, does not agree with the observed magnetic ordering periodicity $0.22\ \pi/c$. This is good evidence that the q dependence of the matrix element is playing an important role in shifting the peak toward a smaller value of q. The peaks for Dy, Er, and Lu all stand out very clearly. The locations of these peaks agree well with the experiments, indicating that the peaks are sharp enough so that they are not much affected by the matrix element. The fact that the peak for Tb is much weaker than those of Dy and Er explains why Tb has a much smaller temperature range of stable helical structure.

The present method of computing $\chi(\vec{q})$ has been used to calculate the pressure dependence of the magnetic ordering properties of Gd, Tb, and Dy.[28] The results are in good agreement with existing experimental data. This demonstrates that the $\chi(\vec{q})$ calculation is sensitive enough to detect rather small pressure shifts.

In Ref. 18, a phenomenological q-dependent matrix element was introduced, i.e.,

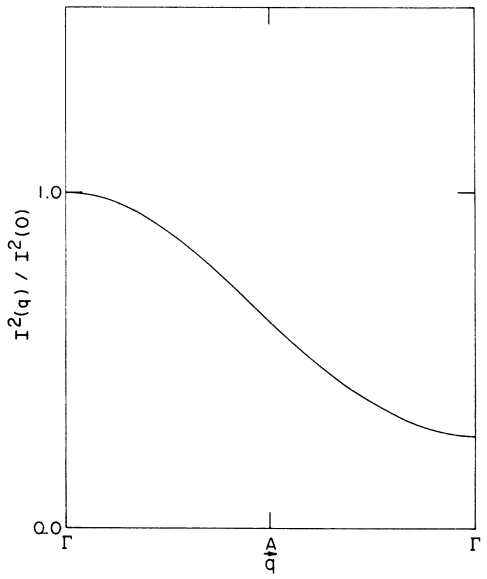

FIG. 12. $I^2(q)/I^2(0)$ for Gd.

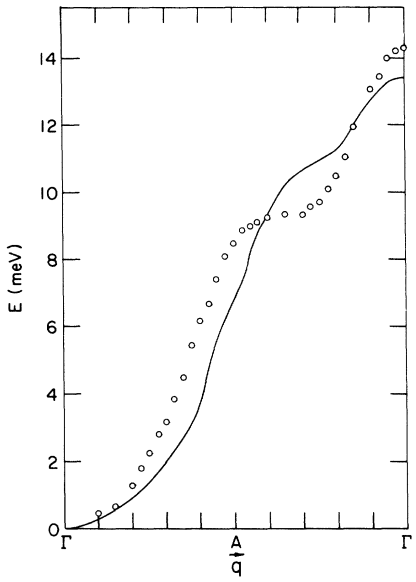

FIG. 13. Spin-wave dispersion curve for Gd.

$$I^2(q) = I^2(0)(e^{-\alpha q^2} + e^{-\alpha(4\pi/c-q)^2}) .$$

Here q denotes the magnitude of $\vec{q}$, which is along the c axis. The parameter $\alpha = 0.05c^2$ is chosen such that the width of $I^2(q)$ corresponds approximately to the width of the $4f$ shell. The size of $I(0)$ must be estimated from other data, such as the conduction-electron polarization. On Fig. 12, we show the q dependence of the matrix element squared. For small q's it has the general shape as that calculated by Watson and Freeman.[27] However, any numerical comparison with their result is probably meaningless because the value of the Fermi wave vector k_F in their calculation is undefined in terms of the real energy bands.

When the $\chi(\vec{q})$ curve is modified by the matrix element, one obtains a curve for $J(\vec{q})$, the Fourier transform of the exchange energy. From this one may calculate the spin-wave spectrum. Figure 13 shows the calculated spin-wave spectrum of Gd compared with the experimental curve at 78 K of Koehler *et al.*[29] In this comparison it is assumed that the magnetic anisotropy and magnetoelastic effects make negligible contributions to the spectrum. The size of the quantity $I(0)$ is determined from the conduction-electron polarization of 0.55 μ_B per atom and the theoretical density of states, 26.8 states per rydberg. These give a conduction-electron band splitting of 0.019 eV and a matrix element $I(0) = 0.074$ eV. The band-splitting effect is included in the $\chi(\vec{q})$ calculation. Bearing in mind the rough nature of the calculation, one may be gratified that the calculated curve has the same bandwidth and shows the same inflections in the optical branch as the experimental result. The inflection also arises from Fermi-surface nesting as discussed in Ref. 29. Although it is not yet possible to perform a first-principles calculation of the spin-wave spectrum of heavy rare earths, the partial success of the present attempt makes it seem hopeful.

The metals Sc and Y do not belong to the rare-earth series, but they share many of the physical properties with the heavy rare earths. They have the hcp structure and are trivalent. Band calculations[30,31] show that their electronic structures are very similar to Lu. We include their $\chi(\vec{q})$ curves here for completeness. Although they are not magnetic, their $\chi(\vec{q})$ curves give information about the magnetic structure of their alloys with magnetic rare earths. The latter exhibit a spiral spin structure with a magnetic wave vector $\vec{q}_m = (0, 0, 0.28) \times 2\pi/c$ in the limit of dilute rare-earth concentrations.[32–34] No appreciable change in this value is observed if the rare-earth concentration is varied slightly in the dilute alloy. This is an indication of the fact that the electron energy bands of Sc and Y are very similar to those of the rare earths. We include here the results of Wakabayashi[35] for the $\chi(\vec{q})$ for Sc obtained using the energy bands of Fleming and Loucks.[31] In the case Y, a full-fledged band calculation had to be performed for lack of availability of bands above the Fermi level. A set of 41 reciprocal lattice vectors[36] was used for this purpose and the energy eigenvalues converged to within 0.001 Ry at the high-symmetry points in the Brillouin zone using this set of reciprocal lattice vectors. Only the third and fourth bands, which determine the Fermi surface, were used in the calculation of $\chi(\vec{q})$ since we are primarily interested in the shape of $\chi(\vec{q})$ and since its relative

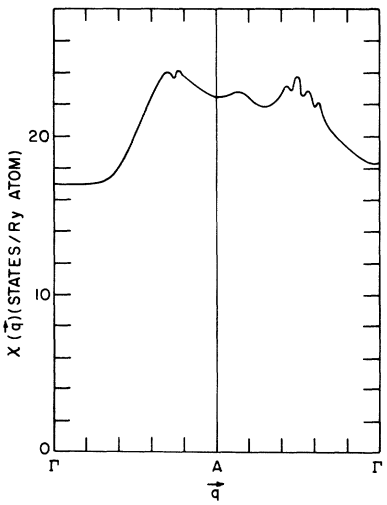

FIG. 14. Generalized susceptibility function for Sc.

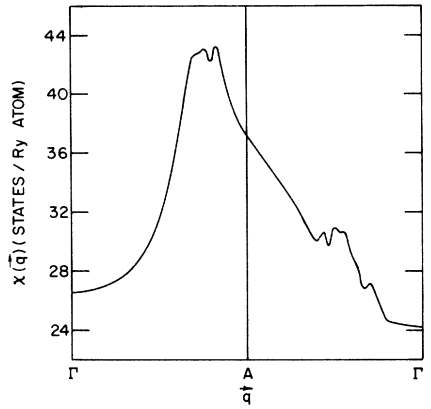

FIG. 15. Generalized susceptibility function for Y.

magnitude is unimportant for us. For both Sc and Y, three broad peaks are obtained (Figs. 14 and 15) roughly positioned at $(0, 0, \xi)2\pi/c$ ($\xi = 0.35, 0.57$, and 0.77 for Sc and 0.375, 0.583, and 0.75 for Y). The position of the first peak in both Sc and Y is quite close to the experimental value of the magnetic wave vector $\vec{q}_m = (0, 0, 0.28)\pi/c$ for their dilute alloys with rare earths.[32–34]

The peaks in $\chi(\vec{q})$ also play an important role in determining the Kohn-type anomalies in the phonon spectra of metals. The dielectric function of a metal which describes the self-consistent screening of the ionic motion by the electrons depends on $\chi(\vec{q})$. The dielectric function is an important quantity and governs the electronic contribution to the

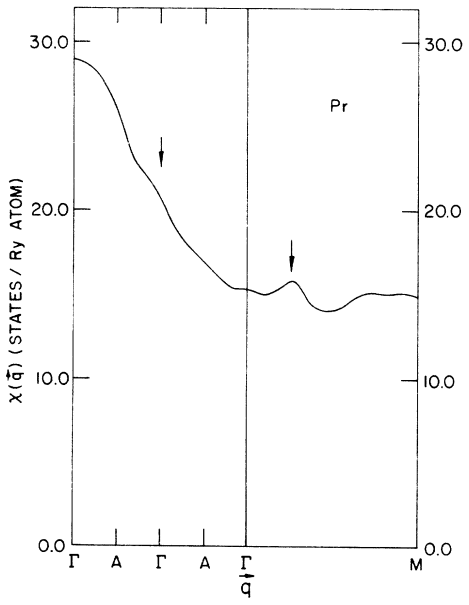

FIG. 16. Generalized susceptibility function for Pr.

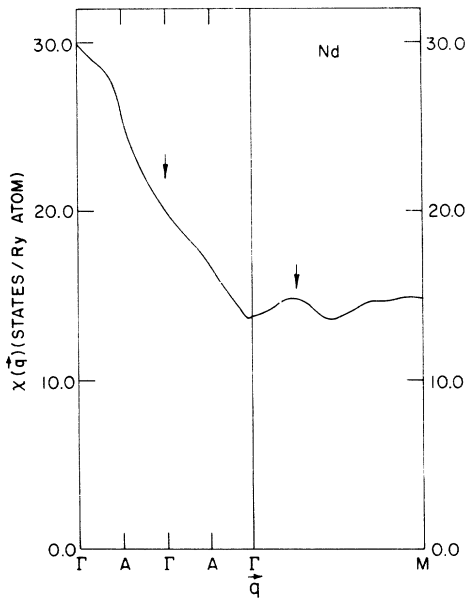

FIG. 17. Generalized susceptibility function for Nd.

dynamical matrix which determines the phonon spectrum. It is believed that the kinks in the phonon dispersion curves arise owing to the peaks in $\chi(\vec{q})$. The dispersion curves of Sc and Y have recently become available due to work of the neutron-scattering group in Ames. In the case of Sc, a kink in the longitudinal acoustic (LA) branch at a wave vector $\vec{q} = (0, 0, 0.27)2\pi/c$ was observed by Wakabayashi, Sinha, and Spedding.[35,37] This is nearly equal to the observed value of the magnetic wave vector,[32,33] and close to the first peak in $\chi(\vec{q})$. No other kinks corresponding to the two other broad peaks in $\chi(\vec{q})$ could be found. For yttrium, on the other hand, no anomalies in the dispersion curves near the first peak in $\chi(\vec{q})$ were detected by Sinha *et al.*,[38] but they reported two sharp dips in the longitudinal optic (LO) branch at positions $(0, 0, 0.625)2\pi/c$ and $(0, 0, 0.775)2\pi/c$ which are in fact very close to the second and third broad peaks in $\chi(\vec{q})$ [$\vec{q} = (0, 0, 0.583)2\pi/c$ and $(0, 0, 0.75)2\pi/c$]. Considering the similarity between the electronic structures of Sc and Y this behavior is unexpected. One indeed expected the Kohn anomalies in both the metals to be observed roughly at the same positions. It is extremely difficult to find a conclusive answer for such a difference at present. The form of the dynamical matrix is much too complicated to determine the relative importance of each peak. For a quantitative answer one will have to calculate the dynamical matrix which depends on the knowledge of accurate wave functions, using a $\chi(\vec{q})$ which also includes the matrix elements. This has not been done so far. For details, the reader is referred to the article by Sinha.[39] It is encouraging

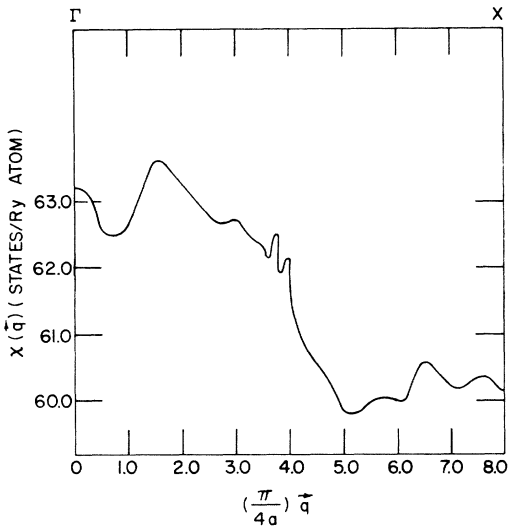

FIG. 18. Generalized susceptibility function for Th along [100] direction.

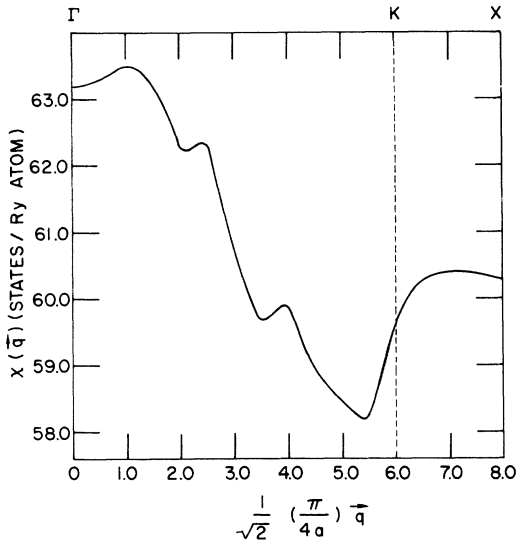

FIG. 19. Generalized susceptibility function for Th along [110] direction.

to note, nevertheless, that there are some important differences in the shape of the $\chi(\vec{q})$ curve of Sc and Y, indicating that a proper calculation of the dynamical matrix may support the experimentally observed structure in the phonon dispersion curves of these two metals.

IV. LIGHT RARE EARTHS

In Refs. 20 and 40, the periodicity of the magnetic structure of dhcp Pr and Nd was shown to be connected with the Fermi-surface nesting features along the $\vec{b}_1$ axis. The periodicity along the $\vec{b}_3$ axis was not understood. We have since detected an error in the $\chi(\vec{q})$ calculation along the $\vec{b}_3$ axis and have repeated the calculation on a mesh described in Sec. II. The results along the $\vec{b}_1$ and $\vec{b}_3$ axes are shown in Figs. 16 and 17, where the arrows indicate the locations of the observed magnetic ordering wave vectors. The $\vec{b}_1$ axis results are not substantially different from those published previously, but along the $\vec{b}_3$ axis the $\chi(\vec{q})$ increases steadily with $\vec{q}$, with the maximum occurring at $4\pi/c$. This maximum is not associated with any Fermi-surface feature, but arises from large regions occupied by electrons and holes that are connected by this wave vector. From this information alone one would conclude that the magnetic moments of adjacent layers would make 90° angles with each other. However, the measured turn angle is 180°. The discrepancy may again be due to the matrix-element modification so that the large-q end is drastically reduced, and the maximum actually occurs at $2\pi/c$. If this is the case, it will be an example where the magnetic periodicity is not controlled by nesting Fermi surfaces.

We have also computed $\chi(\vec{q})$ for wave vectors $\vec{q} = (b_m, 0, q)$, where $(b_m, 0, 0)$ corresponds to the maximum of $\chi(\vec{q})$ along the $\vec{b}_1$ axis. The entire $\chi(\vec{q})$ curve lies slightly above that along the $\vec{b}_3$ axis, so it implies that the wave vector for the magnetic ordering lies in the $b_1 b_3$ plane as found experimentally.

The energy bands and the susceptibility function for the fcc Pr have been studied by Myron and Liu.[41] The susceptibility function was calculated on the same mesh as in the thorium case described in Sec. IV.

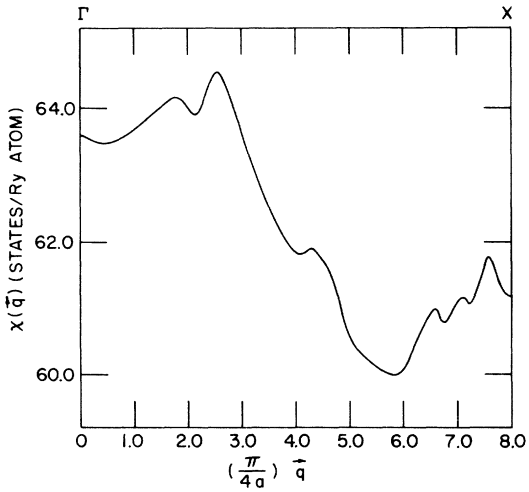

FIG. 20. Generalized susceptibility function for $Th_{0.9}\,RE_{0.1}$ along [100] direction in the rigid-band approximation.

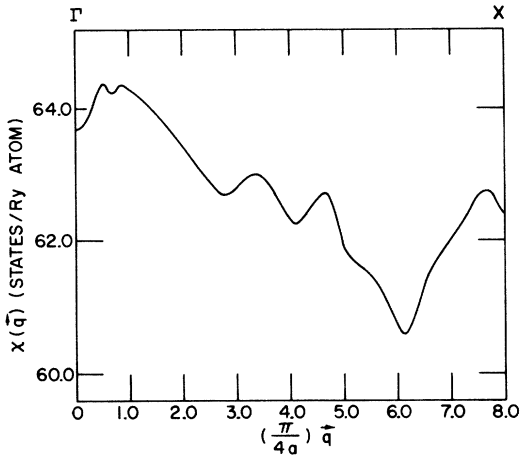

FIG. 21. Generalized susceptibility function for $Th_{0.8}$ $RE_{0.2}$ along [100] direction in the rigid-band approximation.

V. THORIUM AND ITS ALLOYS WITH RARE EARTHS

We have also calculated the $\chi(\vec{q})$ of thorium and also of its alloys with rare earths in varying concentration, all with fcc crystal structure. This work was motivated primarily to investigate the possibility of any magnetic ordering in thorium–rare-earth systems (henceforth referred to as Th-RE). The energy bands of Gupta and Loucks[42,43] were used in this calculation, and only the first three bands were used. The results for thorium in the [100] and [110] directions are shown in Figs. 18 and 19. There are several peaks in the [100] direction. Their origin may be understood in terms of the Fermi surface of thorium. The Fermi surface consists of three distinct closed surfaces: an electron surface centered along ΓK which resembles a pair of lungs in shape, a dumbbell-shaped hole surface centered along ΓL, and a rounded hole cube centered at Γ. The rounded cube has partly flat parallel surfaces separated by a wave vector $q \sim 3.8$ $(\pi/4a)$ in the [100] direction. These flat surfaces give rise to the peak at $q \sim 3.8$ $(\pi/4a)$ shown in Fig. 18. One might expect this peak to be an absolute maximum in $\chi(\vec{q})$ because there are no other obvious flat regions of Fermi surface. This is, however, not the case and a broad maximum at $q \sim 1.6$ $(\pi/4a)$ arises largely due to intraband contributions across the lungs and across the dumbbell. This is because of the peculiar and closed shape of these surfaces. Of course, at $q \sim 3.8$ $(\pi/4a)$ the intraband contribution across the rounded cube dominates. A small peak at $q = 4.0$ $(\pi/4a)$ may be interpreted as arising from the parallel edges of the two electron surfaces. The sharp drop in the curve at $q > 4.0$ $(\pi/4a)$ confirms our interpretation since at these wave vectors the intraband contribution is very small and it is only the interband contribution which is important. The curve in the [110] direction is a little more difficult to interpret but there again one would find that the intraband contributions are important at lower q's while the interband contributions determine the shape of the curve at higher wave vectors. The peaks in the susceptibility function also play an important role in determining the position of the Kohn anomalies in phonon spectra, as discussed in Sec. III in connection with Sc and Y. Reese *et al.*[44] have indeed found a Kohn anomaly corresponding to one of the peaks in the [110] direction, while anomalies corresponding to other

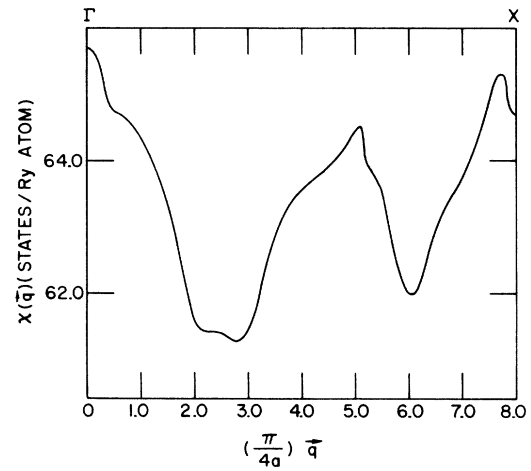

FIG. 22. Generalized susceptibility function for $Th_{0.7}$ $RE_{0.3}$ along [100] direction in the rigid-band approximation.

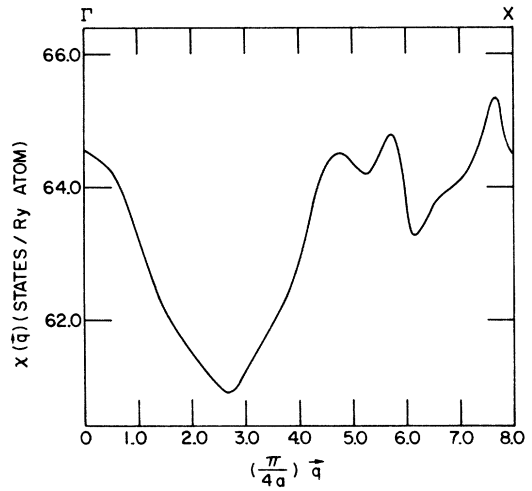

FIG. 23. Generalized susceptibility function for $Th_{0.6}$ $RE_{0.4}$ along [100] direction in the rigid-band approximation.

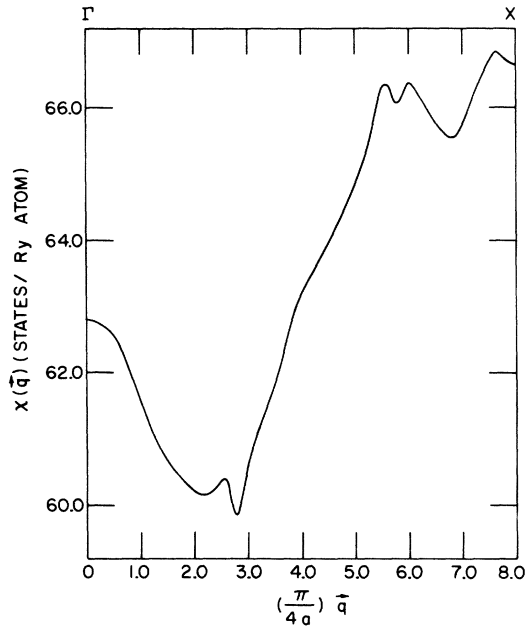

FIG. 24. Generalized susceptibility function for $Th_{0.5}$ $RE_{0.5}$ along [100] direction in the rigid-band approximation.

peaks could not be found.

The calculation for the $Th_{1-x}RE_x$ systems was confined to the [100] direction only. This is because most systems in the ordered state prefer to choose the direction of the highest symmetry for the magnetic wave vector. The calculation was performed assuming that the rigid-band approximation holds. The results are shown in Figs. 20–24 for x varying from 0.1 to 0.5. The only experimental data available on such alloy systems are those of Child *et al.*[45] who carried out the neutron diffraction study of some of the alloys of Th with Tb, Ho, and Er, all having the fcc structure, with the concentration of the rare-earth component being as high as 50 at.%. This work was done in the powder phase and not on single crystals with temperatures ranging from room temperature to 1.3 K. In each case the diffraction pattern at low temperatures exhibited broad diffuse maxima due to magnetic scattering. These diffraction patterns were interpreted in terms of short-range antiferromagnetic correlations. They chose $Th_{0.7}Tb_{0.3}$ alloy as an example for illustration. In this typical case a broad maximum at a scattering angle of about 0.3 of the nuclear (111) reflection and a small hump at about 0.8 of the same reflection were observed. The intensity in the first hump decreased rapidly with temperature up to 39 K, beyond which it tailed off gradually to zero. No significant change in the form of the hump with changing temperature was observed and the intensity in the hump was found never to saturate. The latter are indeed uncharacteristic of the long-range order but resemble very much the behavior found in systems with short-range order. Assuming that the short-range order is present, one can calculate the magnitudes of the magnetic wave vectors corresponding to the positions of the two humps. One finds $Q_1 = 4.13 \times (\pi/4a)$ for the first hump and $Q_2 = 10.93\ (\pi/4a)$ for the second hump. From the powder work, it is not possible to determine the direction of the magnetic wave vector but if it is taken to be the [100] direction, then the two vectors Q_1 and Q_2 in the reduced-zone scheme would correspond to $4.13\ (\pi/4a)$ and $5.07\ (\pi/4a)$, respectively. It is encouraging to note that in our calculation (Fig. 22) a sharp peak at $q_2 = 5.1\ (\pi/4a)$ and a broad peak at $q_1 \sim 3.8\ (\pi/4a)$ are indeed obtained although neither of the two is an absolute maximum. The exact locations of these peaks and their relative magnitudes are, however, unimportant because the conclusions drawn from our calculation may only be qualitatively correct. One should not expect to be able to extract quantitatively accurate information using the rigid-band model with the rare-earth concentration being as high as 30 at.%.

---

*Work performed in part in the Ames Laboratory of the U.S. AEC, contribution No. 2948.

[1]W. C. Koehler, J. Appl. Phys. 36, 1078 (1965).
[2]M. A. Ruderman and C. Kittel. Phys. Rev. 96, 99 (1954).
[3]T. Kasuya, Progr. Theoret. Phys. (Kyoto) 16, 45 (1956).
[4]K. Yosida, Phys. Rev. 106, 893 (1957).
[5]R. J. Elliott, in *Magnetism*, Vol. II A, edited by G. T. Rado and H. Suhl (Academic, New York, 1965), p. 385.
[6]T. Kasuya, in *Magnetism*, Vol. II B, edited by G. T. Rado and H. Suhl (Academic, New York, 1966), p. 215.
[7]D. C. Mattis, *The Theory of Magnetism* (Harper and Row, New York, 1965).
[8]S. H. Liu, Phys. Rev. 123, 470 (1961).
[9]R. J. Elliott and M. F. Thorpe, J. Appl. Phys. 39, 802 (1968).
[10]R. Kubo, J. Phys. Soc. Japan 12, 570 (1957).
[11]J. Villain, J. Phys. Chem. Solids 11, 303 (1959).
[12]J. O. Dimmock and A. J. Freeman, Phys. Rev. Letters 13, 750 (1964).
[13]A. J. Freeman, J. O. Dimmock, and R. E. Watson, Phys. Rev. Letters 16, 94 (1966).
[14]S. C. Keeton and T. L. Loucks, Phys. Rev. 168, 672 (1968).
[15]S. C. Keeton, Ph. D. thesis (Iowa State University, Ames, Iowa, 1966) (unpublished).
[16]L. M. Roth, H. J. Zeiger, and T. A. Kaplan, Phys. Rev. 149, 519 (1966).
[17]W. E. Evenson and S. H. Liu, Phys. Rev. Letters 21, 432 (1968).
[18]W. E. Evenson and S. H. Liu, Phys. Rev. 178, 783 (1969).
[19]W. E. Evenson, Ph. D. thesis (Iowa State University,

Ames, Iowa, 1968) (unpublished).
[20]G. S. Fleming, S. H. Liu, and T. L. Loucks, Phys. Rev. Letters 21, 1524 (1968).
[21]G. S. Fleming, Ph.D. thesis (Iowa State University, Ames, Iowa, 1968) (unpublished).
[22]R. H. Pennington, *Introductory Computer Methods and Numerical Analysis* (MacMillan, New York, 1965).
[23]K. A. Gschneidner, *Rare Earth Alloys* (Van Nostrand, Princeton, N. J., 1961).
[24]W. B. Pearson, *Handbook of Lattice Spacings and Structures for Metals* (Pergamon, New York, 1962).
[25]R. M. Moon, J. W. Cable, and W. C. Koehler, J. Appl. Phys. Suppl. 35, 1041 (1964).
[26]J. W. Cable, R. M. Moon, W. C. Koehler, and E. O. Wollan, Phys. Rev. Letters 12, 553 (1964).
[27]R. E. Watson and A. J. Freeman, Phys. Rev. 152, 566 (1966).
[28]G. S. Fleming and S. H. Liu, Phys. Rev. B 2, 164 (1970).
[29]W. C. Koehler, H. R. Child, R. M. Nicklow, H. G. Smith, R. M. Moon, and J. W. Cable, Phys. Rev. Letters 24, 16 (1970).
[30]T. L. Loucks, Phys. Rev. 144, 504 (1966).
[31]G. S. Fleming and T. L. Loucks, Phys. Rev. 173, 685 (1968).
[32]H. R. Child and W. C. Koehler, J. Appl. Phys. 37, 1353 (1966).
[33]H. R. Child and W. C. Koehler, Phys. Rev. 174, 562 (1968).
[34]W. C. Koehler, H. R. Child, E. O. Wollan, and J. W. Cable, J. Appl. Phys. 34, 1335 (1963).
[35]N. Wakabayashi, Ph.D. thesis (Iowa State University, Ames, Iowa, 1969) (unpublished).
[36]T. L. Loucks, *Augmented Plane Wave Method* (Benjamin, New York, 1967).
[37]N. Wakabayashi, S. K. Sinha, and F. H. Spedding, Phys. Rev. B (to be published).
[38]S. K. Sinha, T. O. Brun, L. D. Muhlestein, and J. Sakurai, Phys. Rev. B 1, 2430 (1970).
[39]S. K. Sinha, Phys. Rev. 169, 477 (1968).
[40]G. S. Fleming, S. H. Liu, and T. L. Loucks, J. Appl. Phys. 40, 1285 (1969).
[41]H. W. Myron and S. H. Liu, Phys. Rev. B · 2414 (1970).
[42]R. P. Gupta and T. L. Loucks, Phys. Rev. Letters 22, 458 (1969).
[43]R. P. Gupta and T. L. Loucks, Phys. Rev. B 3, 1834 (1971).
[44]R. A. Reese, S. K. Sinha, and D. T. Peterson, Phys. Rev. B (to be published).
[45]H. R. Child, W. C. Koehler, and A. H. Millhouse, J. Appl. Phys. 39, 1329 (1970).

PHYSICAL REVIEW B VOLUME 4, NUMBER 4 15 AUGUST 1971

Correlation Factors for Diffusion in Nondilute Alloys

John R. Manning
Metallurgy Division, Institute for Materials Research, National Bureau of Standards, Washington, D. C. 20234
(Received 23 October 1970)

Correlation factors for diffusion in binary and multicomponent alloys are calculated for a random-alloy model with diffusion by a vacancy mechanism. This model, which should apply best for nondilute alloys, assumes that atoms and vacancies are randomly distributed and that suitable average values can be used to represent the actual atom and vacancy jump frequencies in the crystal. In alloys, both atoms and vacancies follow correlated walks. Also, the atom correlation factors are influenced by the nonrandom motion of the vacancies. Thus, in order to treat correlation effects in concentrated alloys properly, one must consider not only the correlation factors f_i for diffusion of atoms but also the correlation factor f_v for diffusion of vacancies. In specific calculations, one also must find the partial correlation factors f_v^i for diffusion of vacancies by exchange with atoms of the particular species i. Analytic expressions for all of these correlation factors are calculated. These equations can be expressed directly in terms of the measureable tracer-diffusion-coefficient ratios D_i^*/D_k^* with no unknown jump frequencies appearing. The calculations also yield a forbidden region in the plot of diffusion-coefficient ratio as a function of alloy composition, with correlation factors going to zero at the boundary of this region. Specific applications to binary alloys are discussed.

INTRODUCTION

When diffusion occurs by a random walk, the diffusion coefficient D_i^* for species i in a cubic crystal is given by

$$D_i^* = \tfrac{1}{6}\lambda^2 \nu_i \,, \tag{1}$$

where λ is the jump distance and ν_i is the jump frequency for species i. When there is a correlated walk, this expression becomes

$$D_i^* = \tfrac{1}{6}\lambda^2 \nu_i f_i \,, \tag{2}$$

where f_i is the correlation factor for species i. Here f_i takes into account the correlation between the directions of successive atom jumps. In crystals having sufficient symmetry and with diffusion by a vacancy mechanism, the general expression for f_i is[1,2]